AIChE

# Impact of Deposit Aging and Surface Roughness on Thermal Fouling: Distributed Model

**F. Coletti**
Dept. of Chemical Engineering and Chemical Technology, Imperial College London, South Kensington Campus, London SW7 2AZ, U.K

**E. M. Ishiyama, W. R. Paterson, and D. I. Wilson**
Dept. of Chemical Engineering and Biotechnology, University of Cambridge, New Museums Site, Pembroke Street, Cambridge CB2 3RA, U.K

**S. Macchietto**
Dept. of Chemical Engineering and Chemical Technology, Imperial College London, South Kensington Campus, London SW7 2AZ, U.K

*DOI 10.1002/aic.12221*
*Published online May 4, 2010 in Wiley Online Library (wileyonlinelibrary.com).*

*A kinetic model was recently proposed to describe the effect of aging on deposit thermal conductivity and the thermal performance of a shell-and-tube heat exchanger undergoing crude oil fouling. The model is adapted for implementation within a dynamic, distributed system with spatial and temporal distributions, relaxing several of the previous assumptions. The evolution of surface roughness is also considered, using conjectural linear and asymptotic functions. Simulations are performed for a single tube representative of a refinery exchanger. The results demonstrate the substantial effects over time of aging and roughness on heat transfer and pressure drop. Roughness effects yield apparently negative initial fouling resistances, as reported in some experimental tests. The importance of accounting for roughness dynamics in short time scale pilot plant scale tests and aging over longer time scales in industrial applications is highlighted.* © 2010 American Institute of Chemical Engineers *AIChE J,* 56: 3257–3273, 2010
*Keywords: aging, crude oil, fouling, mathematical model, roughness*

## Introduction

Fouling of heat exchangers is an expensive and ongoing problem in the process industries: it results in substantial additional costs due to reduced thermal and hydraulic efficiency, reduced throughput, periodic cleaning, increased external utility requirements and additional $CO_2$ emissions. Its economic impact has been well documented.[1–4] The formation of fouling deposits can occur via different mechanisms, as outlined by Epstein,[5] some of which can occur in parallel. Figure 1 shows some of the subprocesses identified by Epstein: the phenomena involved often interact, regardless of the mechanism(s), so that it is often difficult to interpret observations in simple terms.

The deposition of foulant material on heat-transfer surfaces often results in a progressive increase in roughness and narrowing of ducts/pipes, with associated effects on heat-transfer coefficient and pressure drop. Deposits may undergo structural changes over time (aging) that can affect the overall dynamic behavior of the system. The exposure of the fouling layer to wall temperatures over extended periods can trigger chemical transformations which alter the structure

Correspondence concerning this article should be addressed to S. Macchietto at s.macchietto@imperial.ac.uk.

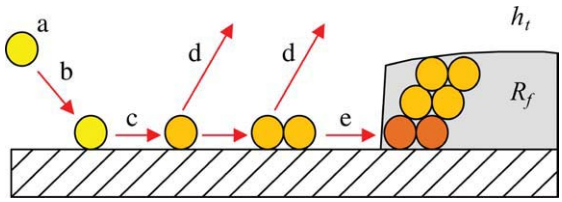


**Figure 1. Schematic of subprocesses involved in fouling on a heat transfer surface, as proposed by Epstein.[5]**

(a) Formation of fouling precursors, (b) transport to surface, (c) attachment, (d) removal, and (e) aging. Once the fouling layer is formed its thermal resistance $R_f$, and the convective film heat-transfer coefficient, $h_t$ govern heat transfer. [Color figure can be viewed in the online issue, which is available at wileyonlinelibrary.com.]

and properties of the deposit. As an example, Nelson's early model of crude oil fouling described initial deposition as involving a gel which changes its structure over time to a harder material similar to coke.[6,7] This not only alters the rheology of the deposit layer,[8] but also its thermal conductivity, and, thus, the thermohydraulic behavior of the exchanger. Within a fouling layer the material is subject to a range of temperature histories so that aging is nonuniform in space and highly time-dependent. Despite the importance of these effects, relatively little attention has been paid in the literature to these phenomena, particularly in the area of chemical reaction fouling. A summary of previous work in that area was given by Ishiyama et al.[9] and also this article follows on from that study.

Ishiyama et al.[9] developed a kinetic model for aging in chemical reaction fouling, extending the two-layer model proposed by Crittenden and Kolaczkowski.[10] The focus of their work was on crude oil fouling, as found in a refinery preheat train. In that article, we presented a parametric study which showed the importance of considering aging when interpreting fouling data from experiments, and modeling the fouling behavior of industrial units. The model quantified aging via its impact on deposit thermal conductivity, and the article explored the influence of different temperature dependencies and time scales between the deposition and aging subprocesses. A summary of its key features is presented in Table 1.

That work provides a useful framework for assessing the impact of aging on the performance of industrial heat exchangers, and demonstrated the importance of considering aging in laboratory tests, where accelerated conditions are often employed to reduce test durations. However, the model as presented is a point or aggregate (lumped) model, that is, it does not consider the variation in conditions across a heat exchanger. Furthermore, it uses a number of simplifying assumptions such as the thin-slab assumption for the overall resistance of the fouling layer, which is only valid when the maximum thickness of the fouling layer is about 10% of a typical inner tube diameter for the shell-and-tube devices used in practice.[11] In practice, it is not uncommon for fouling to reduce the diameter available for flow in a tube by more than this amount. Other limitations arose from the numerical solution methodology used, which was essentially an explicit, fixed-step integration of the differential equations. The deposit of each new layer was assumed to occur at discrete time intervals of fixed duration (one day in the article). Also, a simplified form of the fouling model was used.

The aforementioned simplifications did not affect the general form of the results, but do need to be considered in detailed modeling. In this article, we extend the model of Ishiyama et al.[9] to a long tube as found in shell-and-tube heat exchangers and relax some of its assumptions, as detailed in Table 1. A more general fouling model is considered which includes variation in local conditions, time, and nature of the deposit layer. The fouling layer is treated as a moving boundary domain which varies in thickness over time, depending on process conditions. The model is

**Table 1. Assumptions in the Ishiyama et al.[9] Model Relaxed in this Article**

| Assumption | Limitation | This paper | Benefits |
|---|---|---|---|
| No suppression term in fouling model | No suppression mechanism considered | Suppression term introduced in the fouling model | More realistic description captures the interaction between fouling layer and wall shear stress |
| Thin–slab assumption for thermal resistance of deposit layer, $R_f$ | Estimate of $R_f$ inaccurate when deposit thickness >10% $d_o$ | Moving boundary problem in cylindrical coordinates | Faster fouling rates can be considered. No limitations on the deposit thickness, including large pipe occlusions |
| Fixed layer deposition time | Layers start ageing at fixed time intervals | Layer growth dependant on fouling rate. | More realistic description in case of linear deposition rate. |
| Lumped model | No axial profiles of model variables | Distributed over length (all domains) and radial coordinate | Axial and radial phenomena can be tracked |
| Constant roughness | Negative fouling resistance not captured | Model proposed for roughness dynamics | Explains 'apparent' negative fouling resistance *via* initial heat transfer enhancement |
| Full heat exchange model | Point model or averaged across full exchanger | Single tube | May be used to model experimental apparatus and within heat exchangers of various configurations |
| Explicit integration with fixed time steps; sequential solution of equations | Discrete time steps; cannot deal with steep gradients | Fully implicit, simultaneous solution of PDAEs; | Continuous solutions, numerical stability, accuracy; can deal with steep gradients; multiscale phenomena |

formulated in cylindrical coordinates which makes it possible to overcome the thin-slab approximation and account for curvature effects in the heat flux. Through a variable change, detailed in later sections, it was possible to apply the aging model to a distributed system. All equations are solved simultaneously using a state-of-the-art implicit integration method, which automatically accounts for the distinct dynamic responses of various system components.

Hewitt et al.[12] reported that fouling can influence the overall heat-transfer coefficient via three effects, namely:

1) A reduction due to the thermal resistance of the fouling layer;

2) an increase due to the increased local velocity resulting from reduced flow area;

3) a change (usually an increase) in the roughness of the heat-transfer surface.

The effect of fouling on surface roughness has received relatively little attention in the literature. While the surface roughness has little effect on the friction factor and heat-transfer coefficient in laminar flow,[13] it plays an important role in turbulent regime typical of industrial applications. The disruption of the viscous sublayer caused by a rough surface generates an increase in the turbulence level compared to that of smooth surfaces,[14] which in turn produces higher heat-transfer coefficients. A constant value of equivalent sand roughness is typically used, calculated from shorthand correlations. Enhancement of heat transfer due to an initial increase in surface roughness generated in fouling tests has been reported and analyzed for particulate fouling by Crittenden and Alderman,[15] and for crystallization fouling by Albert et al.[16] For chemical reaction fouling, most of the reported cases have been qualitative. Bott[17] noted in 1990 that, due to the complex interaction of variables, no systematic study on the effects of roughness on fouling had been undertaken. However, some quantitative results have been presented. Yeap et al.[11]noted that the apparent negative fouling resistance reported in the initial period (up to 40 h) of testing a crude oil by Knudsen et al.[18] could be attributed to surface roughness. Wilson and Watkinson[19] reported both thermal and hydraulic roughness effects (from analysis of pressure drop measurements) in studies of autoxidation reaction fouling, while Asomaning et al.[20] observed these in testing crude oils. Quantitative modeling is in its infancy: for example, in their analysis of crude oil heat exchangers subject to fouling, Yeap et al.[21] changed the surface roughness of clean tubes to that reported for bitumen by Kern[22] to represent the foulant. An approach to model the increase in roughness due to fouling on tube surfaces was developed by Yiantsisio and Karabelas.[23] They proposed a population balance model based on a population of roughness elements to describe deposition and removal in crystallization fouling. However, their focus was on the removal process and they did not discuss roughness in terms of hydrodynamics, pressure drop and more importantly, impact on heat transfer. To the authors' knowledge, no dynamic models exist for roughness effects in chemical reaction fouling, which is related to the paucity of experimental data.

The dynamics of surface roughness are expected to apply mainly to laboratory testing, where more precise measurements of heat transfer are made, over short time scales. Industrial applications feature larger time scales, so that short-term variations in surface roughness are not noticed and the approach adapted by Yeap et al.[21] is expected to suffice. Nonetheless, being able to capture this phenomenon is essential for the correct interpretation of accelerated fouling tests performed in pilot plant.

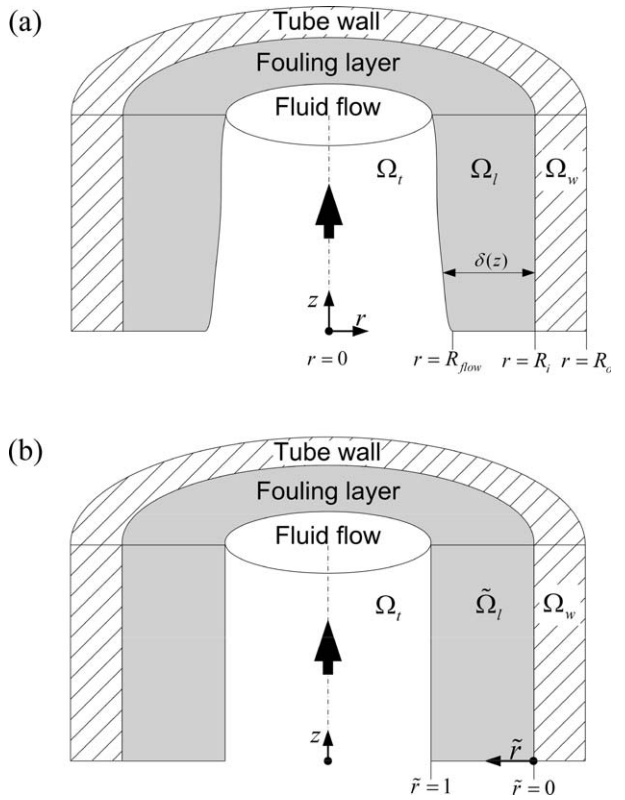


**Figure 2. Definition of domains and reference system in (a) dimensional, and (b) dimensionless coordinate.**

### *System definition*

The model considers fouling on the tube-side of a shell-and-tube heat exchanger, as shown in Figure 2. The dimensions and operating conditions used is representative of those employed in refinery applications. However, the model is readily adapted to other geometries representative of laboratory or pilot plant scale experiments, such as the annular flow configuration used in the HTRI heated rod testing system. The physical system is divided into three domains, as shown in the figure:

$\Omega_w$: The tube wall domain, defined as the region between the inner radius of the tube $R_i$, and its outer radius $R_o$.

$\Omega_l$: The deposit layer domain, defined as that between the crude oil/deposit layer interface (at the flow radius, $r = R_{\text{flow}}$), and the inner radius of the tube $R_i$.

$\Omega_t$: The tube-side flow domain, defined between the tube center ($r = 0$) and $R_{\text{flow}}$.

The model is defined in each domain along the length of the tube (from $z = 0$ to $z = L$). In the deposit layer and tube wall domains ($\Omega_l$ and $\Omega_w$) it is also distributed along the radial coordinate. This allows phenomena which vary in the radial direction, such as the aging of deposit, to be modeled.

The tube-side flow is treated as being locally well-mixed in the radial direction (i.e., in plug flow), as the flow is turbulent and the components in the model are not related to radial variations in the flow domain. Heat-transfer coefficients, for instance, are calculated using established correlations. It should be noted that the location of the fluid/deposit interface $R_{\text{flow}}$, is determined by the deposit thickness and changes along $z$ with time, depending on local fouling conditions.

The physical properties of the crude oil flowing in the tube such as density, $\rho$, dynamic and kinematic viscosities, $\mu$ and $v$, thermal conductivity, $\lambda$ and heat capacity $c_p$, are calculated using API relationships[24] as functions of temperature and space.

Entrance and exit effects in the tube are neglected (i.e., the flow is considered thermally and hydraulically fully developed at $z = 0$). Gravity effects are assumed to be negligible, and symmetry is assumed in the angular coordinate, $\theta$.

Results are presented for two important operating cases, namely (a) uniform wall temperature (UWT), and (b) uniform heat flux (UHF) as reported by Ishiyama et al.[9]

### *Distributed model with moving boundaries for a single tube*

The derivation of the model equations from first principles is reported elsewhere,[25,26] and is not repeated here. In the following sections, the main model equations in each domain are summarized. Two different operating modes, resulting in different boundary conditions, are considered: uniform heat flux (UHF), and uniform wall temperature (UWT).

Equations for the wall and fouling layer domains are written in cylindrical coordinates. No limitations are, therefore, set on the maximum thickness of the fouling layer.

### *Tube wall*

Heat transfer occurs via conduction in domain $\Omega_w$. Assuming constant tube geometry and material properties (wall thermal conductivity $\lambda_w$, density $\rho_w$, and heat capacity $c_{p,w}$), and neglecting phenomena in the axial direction

$$\frac{\rho_w c_{p,w}}{\lambda_w}\frac{\partial T_w(z,r)}{\partial t} = \frac{1}{r}\frac{\partial T_w(z,r)}{\partial r} + \frac{\partial^2 T_w(z,r)}{\partial r^2}; \quad ]R_i, R_0[ \tag{1}$$

where $T_w$ is the local temperature at time $t$ and location ($z$, $r$). The heat flux across the tube wall in the radial direction is calculated as

$$q_w(z,r) = -\lambda_w \frac{\partial T_w(z,r)}{\partial r}; \quad ]R_i, R_0[ \tag{2}$$

### *Deposit layer*

The deposit layer, domain $\Omega_l$, is also modeled as a conductive domain neglecting variations in the axial direction

$$\rho_l c_{p,l}\frac{\partial T_l(z,r)}{\partial t} = \frac{1}{r}\frac{\partial}{\partial r}\left(\lambda_1(z,r) r \frac{\partial T_l(z,r)}{\partial r}\right); \quad ]R_{flow}, R_i[ \tag{3}$$

Here, $T_l$ is the local temperature, and $\lambda_l$ the thermal conductivity, both of which are functions spatial coordinates $r$, $z$ and of time. The density of the deposit layer $\rho_l$ and its heat capacity $C_{p,l}$, are assumed uniform and constant. Equation 3 accounts for the variation of the thermal conductivity in the radial direction. The radial heat flux at any point in the deposit layer is calculated as

$$q_l(z,r) = -\lambda_l(z,r)\frac{\partial T_l(z,r)}{\partial r}; \quad ]R_{flow}, R_i[ \tag{4}$$

Equations 3 and 4 are defined in the domain between $R_i$, and the moving boundary coordinate $R_{\text{flow}}$

$$R_{flow}(z) = R_i - \delta(z) \tag{5}$$

where the deposit thickness $\delta$, is calculated as shown later by Eq. 25.

To solve the set of PDEs with a moving boundary, Eqs. 3 and 4 are reformulated in dimensionless form with respect to the radial coordinate, using a coordinate transformation. The following dimensionless radial coordinate is introduced

$$\tilde{r}\frac{r - R_i}{R_{flow} - R_i} \tag{6}$$

So that

$$\begin{array}{llll} \text{at} & r = R_i & \tilde{r} = 0 & \text{(wall)} \\ \text{at} & r = R_{flow} & \tilde{r} = 0 & \text{(fresh deposit)} \end{array} \tag{7}$$

From the definition of the flow radius in Eq. 5, the new radial coordinate can also be written as

$$\tilde{r} = \frac{R_i - r}{\delta(z)} \tag{8}$$

Figure 2b shows a schematic of the deposit domain coordinate transformation between $\Omega_l$ and the dimensionless domain $\tilde{\Omega}_l$. In terms of the new radial coordinate, Eq. 3 becomes

$$\delta(z)^2\rho_l c_{p,l}\frac{\partial T_l(z,\tilde{r})}{\partial t} = \frac{\partial \lambda_l(z,\tilde{r})}{\partial \tilde{r}}\frac{\partial T}{\partial \tilde{r}} - \frac{\lambda_l(z,\tilde{r})\delta(z)}{R_i - \tilde{r}\delta(z)}\frac{\partial T_l(z,\tilde{r})}{\partial \tilde{r}} + \lambda_l(z,\tilde{r})\frac{\partial^2 T_l(z,\tilde{r})}{\partial \tilde{r}^2} \tag{9}$$

Similarly, Eq. 4 becomes

$$q_l(z,\tilde{r}) = \frac{\lambda_l(z,\tilde{r})}{\partial(z)}\frac{\partial T_l(z,\tilde{r})}{\partial \tilde{r}} \tag{10}$$

### *Aging model*

As noted earlier, exposure of the deposit layer to distinct temperature histories over time causes its structure to change (aging). Aging is principally expressed via a change in the deposit thermal conductivity,[9] between that of the freshly deposited material (the lower limit) $\lambda_l^0$, and a maximum value $\lambda_l^\infty$. In the dimensionless domain we have

$$\lambda_l(z,\tilde{r}) = \lambda_l^\infty + (\lambda_l^0 - \lambda_l^\infty) \times y(z,\tilde{r}) \tag{11}$$

Typical thermal conductivity values[27] are $= 0.2\ \text{Wm}^{-1}\ \text{K}^{-1}$ (initial gel-like deposit, $\lambda$ similar to oil), and $\lambda_l^\infty = 1\ \text{Wm}^{-1}\ \text{K}^{-1}$

(coked deposit). These values were employed in the simulations presented here.

The "youth" variable $y$, introduced by Ishiyama et al.[9] is calculated assuming first-order exponential decay dynamics defined by

$$\frac{dy(z,\tilde{r})}{dt_{age}} = -A_a \exp\left(-\frac{E_a}{R_g T_l(z,\tilde{r})}\right) \times y(z,\tilde{r}) \qquad (12)$$

where $E_a$ and $A_a$ are, respectively, the activation energy (i.e., the temperature dependency), and pre-exponential constant characteristic of the aging process. It should be noted that aging is very sensitive to the local deposit temperature $T_l$.

The aging time $t_{age}$, in Eq. 12 refers to the lifetime of the deposit, and, therefore, depends on when it was formed. For an element formed at instant $t_A$

$$t_{age} = t - t_A \quad \forall t \geq t_A \qquad (13)$$

Each element of deposit in a deposit layer will feature a particular lifespan, between 0 and $t$, which needs to be tracked through time to evaluate the change in $y$. This task represents a form of population balance. Ishiyama et al.[9] captured these dynamics by discretizing the layer into elements formed at regular time intervals and integrating Eq. 12 for each element, via a series of ODEs.

Here we present a continuous formulation that captures the age of individual elements in the fouling layer, which is exact for the particular case of constant deposition rate, i.e., the deposit thickness increases linearly with time. This corresponds to the condition expected for fouling experiments performed under conditions of constant heat flux (and no change in surface roughness), and we show later that it represents a conservative estimate for the other commonly used experimental mode, of uniform wall temperature.

Consider the case of deposit growing at constant rate, as shown in Figure 3a. At time $t_{\mathrm{I}}$ the deposit has grown to a thickness $\delta_{\mathrm{I}}$, and the age of the fresh deposit is zero. The radial location of the element of fresh deposit is $R_{\mathrm{flow}}$, and, thus, $\tilde{r} = 1$. At time $t_{\mathrm{II}}$ the deposit layer has grown to overall thickness $\delta_{\mathrm{II}}$. The age of the deposit formed at time $t_{\mathrm{I}}$ is now $t_{\mathrm{II}} - t_{\mathrm{I}}$, which by similar triangles is given by

$$t_{age} = t_{II}\left(\frac{\delta_{II} - \delta_I}{\delta_{II}}\right) - t_{II} \times (1 - \tilde{r}) \qquad (14)$$

A general relationship between temporal and spatial variables, which applies from the time of formation of the element of deposit, can be written

$$t_{age} = t(1 - \tilde{r}) \qquad (15)$$

Using Eq. 15, the L.H.S. of Eq. 12 may then be rewritten as

$$\frac{dy(z,\tilde{r})}{dt_{age}} = \frac{dy(z,\tilde{r})}{dt}\frac{dt}{dt_{age}} = \frac{dy(z,\tilde{r})}{dt}\frac{d}{dt_{age}}\left(\frac{t_{age}}{1-\tilde{r}}\right) \qquad (16)$$

Hence

$$\frac{dy(z,\tilde{r})}{dt_{age}} = \frac{1}{1-\tilde{r}}\frac{dy(z,\tilde{r})}{dt} \qquad (17)$$

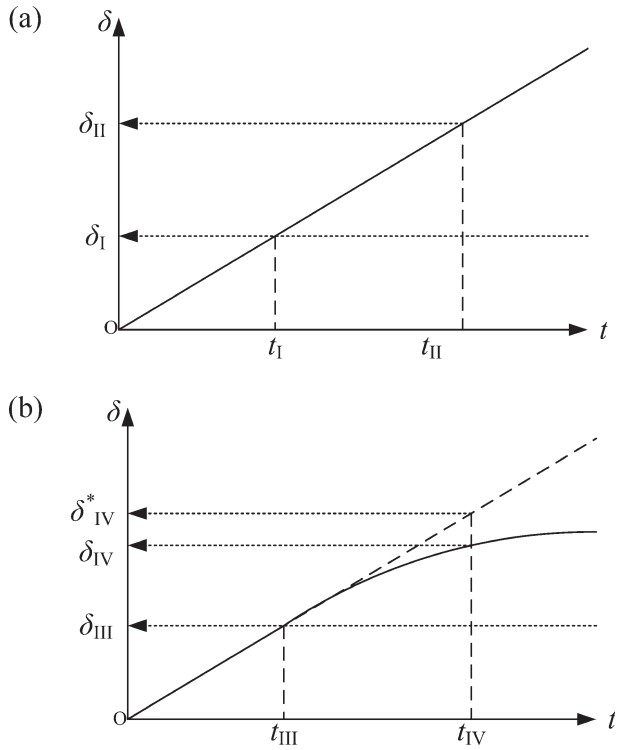


**Figure 3. Schematic showing aging time-deposit thickness construction for (a) constant deposition rate, and (b) deposition rate with autoretardation.**

Therefore, Eq. 12 becomes

$$\frac{dy(z,\tilde{r})}{dt} = (1-\tilde{r})\left[-A_a \exp\left(-\frac{E_a}{R_g T_l(z,\tilde{r})}\right) \times y(z,\tilde{r})\right] \qquad (18)$$

Differential Eq. 18 is expressed in the same time coordinate as the other differential equations and, can, therefore, be integrated simultaneously with them.

When the deposition rate (here, referring to the change in deposit thickness) is not constant, the aging transformation (Eq. 15) is not exact. Consider the autoretardation (falling rate) scenario in Figure 3b. The age of the deposit element formed at instant $t_{\mathrm{III}}$ at time $t_{\mathrm{IV}}$ is $(t_{\mathrm{IV}} - t_{\mathrm{III}})$. The deposit layer has grown to thickness $\delta_{\mathrm{IV}}$, which is smaller than that given by linear growth, $\delta^*_{\mathrm{IV}}$. The dimensionless co-ordinate of the material formed at $t_{\mathrm{III}}$ is $\tilde{r} = \delta_{III}/\delta_{IV}$, which is greater than that given by the linear deposition case $(\delta_{\mathrm{III}}/\delta^*_{\mathrm{IV}})$. The age of this element given by Eq. 15 will be smaller than the true value and Eq. 18 will, therefore, under predict the rate of aging. The transformation, is, therefore, an approximation for this scenario and provides a conservative estimate of the effect of aging. This is considered to be allowable, particularly when the underlying physics and associated parameters are not well known.

Equations 11 and 18 together give the thermal conductivity at each point in the deposit layer undergoing aging, and its use in Eq. 9 gives the temperature evolution in the layer at any time.

### *Tube-side flow*

Deposition inside the tube reduces the cross-sectional area for flow $A_{flow}$, over time and space which depend on the local conditions, affecting both heat transfer and pressure drop along the tube. The variation of the cross-sectional area in domain $\Omega_t$ is included in the enthalpy balance for an element in plug flow

$$\frac{\partial}{\partial t}(\rho c_p T A_{flow}) = -\frac{\partial}{\partial z}(\rho c_p T u A_{flow}) + \frac{\partial}{\partial z}\left(\lambda A_{flow}\frac{\partial T}{\partial z}\right) + 2\pi R_{flow} h_t (T_t(z, R_{flow}) - T) \quad (19)$$

where $T(z)$ is the fluid temperature, and $u(z)$ its mean velocity, which depends on $A_{\text{flow}}$ The local film heat-transfer coefficient $h_t(z)$, is calculated through Eq. 22. The fluid physical properties density, $\rho(z)$, specific heat capacity $c_p(z)$, and thermal conductivity $\lambda(z)$, are functions of API gravity, mean average boiling point and temperature.

The hydraulic effects of fouling are important, both in terms of the pressure drop across the exchanger and the role of surface shear stress on the rate of fouling (section). The pressure drop along the tube is calculated using

$$\frac{dP(z)}{dz} = C_f \frac{\rho(z) u(z)^2}{r_{flow}(z)} \quad (20)$$

The Fanning friction factor $C_f$, for tubes of roughness $e$, is calculated in the turbulent regime via[28]

$$C_f(z) = \left\{ -1.737 \ln\left[0.269\frac{e(z)}{2R_{flow}(z)} - \frac{2.185}{Re(z)}\ln\left(0.269\frac{e(z)}{2R_{flow}(z)} + \frac{14.5}{Re(z)}\right)\right]\right\}^{-2} \quad (21)$$

The role and importance of the surface roughness are discussed in the section entitled

Both $R_{\text{flow}}$ and the surface roughness (via $C_f$) affect the local tube-side heat-transfer coefficient $h_t$. This is accounted for in the correlation[29]

$$h_t(z) = \left(\frac{\lambda(z)}{2R_{\text{flow}}(z)}\right)\frac{\left(\frac{c_f(z)}{2}\right)(Re(z) - 1000)Pr(z)}{1 + 12.7\sqrt{\frac{c_f(z)}{2}}(Pr(z)^{0.67} - 1)} \quad (22)$$

where $Re$ and $Pr$ are the local Reynolds and Prandtl numbers, respectively, evaluated at the bulk temperature. For a given mass flow rate, Eq. 22 shows that $h_t$ is enhanced by a progressive reduction in cross-sectional area, showing that fouling can have a positive effect on heat transfer albeit at the expense increased pressure drop.

An average convective heat-transfer coefficient is defined as

$$\bar{h_t} = \frac{1}{L}\int_0^L h_t(z)dz \quad (23)$$

which will be used in the next section to calculate an overall heat-transfer coefficient.

### *Fouling model*

Chemical reaction fouling, particularly in the area of crude oil fouling as considered here, is complex. There are presently no theoretical models that can reliably describe the inception, growth (and where applicable, removal) of chemical reaction fouling layers from first principles. Several semiempirical models have been proposed to calculate the fouling resistance as a function of process conditions and time. We employ here one of the so-called "threshold fouling" models (a term coined by Ebert and Panchal[30]) to describe the local fouling rate, where the thermal impact of fouling is modeled as a competition between a strongly temperature-dependent "deposition" term, and a "suppression" term related to surface shear stress. Panchal et al.[31] proposed the following correlation for the thermal fouling rate, where $R_f$ is the thermal resistance to heat transfer of the fouling layer

$$\frac{dR_f(z)}{dt} = \alpha Re(z)^{-0.66} Pr(z)^{-0.33}\exp\left(\frac{-E_f}{R_g T_f(z)}\right) - \gamma\tau(z) \quad (24)$$

Here $T_f$ is the film temperature and $\tau$ the shear stress on the deposit-interface. It should be noted that this approach differs from the Kern-Seaton[32] model that yields asymptotic fouling behavior in that the suppression term only affects the increase in $R_f$ : there is no "removal" mechanism acting. Here $\alpha$, $\gamma$, and the fouling activation energy $E_f$, are adjustable parameters that vary between different crudes.

This model is typically used to give an aggregate fouling resistance over a whole heat exchanger, with parameters adjusted to fit overall thermal balances based on measured temperatures and flows. In this work, the aforementioned fouling model is used to calculate the rate of deposition, at each point along the axial direction, based on local conditions. The increase in fouling layer thickness can be calculated knowing the thermal conductivity of a newly deposited layer, which is taken to be $\lambda_l^0$, being that of an oily gel as discussed in the section entitled Introduction

$$\frac{d\delta(z)}{dt} = \lambda_t^0 \frac{dR_f(z)}{dt} \quad (25)$$

Integration of Eq. 25, together with the other model equations, allows calculation of the deposit thickness and flow radius $R_{flow}$, at each point along the axis.

The standard method to represent the thermal effect of fouling is by means of an overall "fouling resistance". We may use the detailed, distributed information on thermal conductivity at each point in the fouling layer to compute what we may define an average fouling resistance, viz

$$\bar{R_f} = \frac{1}{L}\int_o^L\left(\int_o^1 \frac{\delta(z)}{\lambda_l(z,\tilde{r})}d\tilde{r}\right)dz \quad (26)$$

Although the distributed information is useful for identifying and analyzing performance at different allocations in the tube, the average fouling resistance defined in Eq. 26 can be used to assess the overall thermal performance of a tube

**Table 2. Summary of Main Geometric, Physical Property and Operational Model Parameters**

| Parameter | Symbol | Units | Value |
|---|---|---|---|
| Tube length | $L$ | m | 6.1 |
| Outer tube diameter | $d_o$ | mm | 25.4 |
| Inner tube diameter | $d_i$ | mm | 22.9 |
| Minimum roughness | $e^0$ | $\mu$m | 10 |
| Maximum roughness | $e^\infty$ | $\mu$m | 150 |
| Inlet temperature | $T_{\text{in}}$ | °C | 250 |
| Mass flowrate | $\dot{m}$ | kg $s^{-1}$ | 0.3 |
| Inlet pressure | $P_{\text{in}}$ | bar | 30 |
| Uniform wall temperature | $T_0$ | °C | 270 |
| Crude gravity | °API | °API | 37 |
| Crude density at 250°C | $\rho$ | kg $m^{-3}$ | 680 |
| Crude mean average boiling point | MeABP | °C | 350 |
| Crude specific heat at 250°C | $C_p$ | J $kg^{-1}$°$C^{-1}$ | 2916 |
| Crude Kinematic viscosity at 100°F (37.78°C) | $v_0$ | Cs | 4 |
| | | $m^2s^{-1}$ | $4 \times 10^{-6}$ |
| Universal gas constant | $R_g$ | J $K^{-1}mol^{-1}$ | 8.314 |

undergoing fouling. The overall heat-transfer coefficient $U$, is defined as

$$\frac{1}{UA_0} = \frac{1}{A_i}\frac{1}{\bar{h}_t} + \frac{\bar{R}_f}{A_i} + \frac{1}{A_m}\frac{\delta_w}{\lambda_w} \tag{27}$$

where $\delta_w$ is the wall thickness $A_o$ is the outer surface area of the tube $A_i$ the inner one and $A_m$ is the logarithmic mean area. The average fouling resistance defined in Eq. 26 can be compared against other aggregate ways of calculating it. In current practice, $\bar{R}_f$ is estimated from heat balances on the exchanger

$$\begin{aligned}\frac{1}{U} &= \frac{1}{U_{clean}} + \bar{R}_f \\ &= \frac{F \times A \times \Delta T_{lm}}{Q}\end{aligned} \tag{28}$$

where $A$ is the area for heat transfer, $Q$ the heat duty, $\Delta T_{lm}$ the log-mean temperature difference, and $F$ the correction factor.

### *Surface roughness dynamics*

To account for the effect of the increase in roughness given by fouling deposition on heat transfer, two functional forms for the roughness $e$ in Eq. 21 are proposed.

Surface roughness is often expressed in terms of an equivalent sand roughness[33] $e$: typical values for clean, tubes range[34] from 1.5 $\mu$m (for drawn steel tubes) to 46 $\mu$m, whereas that of bitumen layers has been reported[22] as 120 $\mu$m. Although chemical reaction fouling is often accompanied by observable changes in surface roughness (see the references in the Introduction, and Yang et al.[35]), there are currently no established models to calculate surface roughness of chemical reaction fouling deposits from first principles and indeed there are few data available. Here, surface roughness dynamics is modeled as increasing from a minimum value (that of a clean tube) $e^0$, as deposition increases until a maximum value, $e^\infty$ is reached. Values used for simulations are reported in Table 2.

In the absence of experimental data, two hypothetical models are considered to illustrate the effect. The first is a simple linear ramp related to the thickness of the fouling layer

$$e = e^0 + \min(k_p\delta, e^\infty) \tag{29}$$

where $k_p$ is a rate constant. When the maximum value $e^\infty$, is reached, the roughness does not change anymore. This introduces a mathematical discontinuity which is unlikely to occur in reality (see results in the Impact of surface roughness dynamics section, and Figure 5a). It is acknowledged that this is a simple model, which suggests that deposition occurs via the buildup a uniform layer, the surface of which increases in roughness. The change in deposit thickness $\delta$, is calculated from the thermal fouling model (Eq. 22), which does not, however, include roughness effects. Therefore, there is considerable scope for development of these dynamic models.

A second model treats the surface roughness as evolving asymptotically over time to its final value (with $k_t$ the time it takes to achieve half of the final roughness)

$$e = e^0 + (e^\infty - e^0)\frac{t}{t + k_t} \tag{30}$$

However, if deposition does not occur, the roughness should not change. For this reason, a different model, although exhibiting the same asymptotic behavior of Eq. 30, is proposed to relate the roughness to the thickness of the fouling layer

$$e(z) = e^0 + (e^\infty - e^0)\frac{\delta(z)}{\delta(z) + k_a e^\infty} \tag{31}$$

Equation 31 states that the roughness of the interface between oil and deposit layer evolves asymptotically from the clean tube value $e^0$, to a final value $e^\infty$, characteristic of the deposit type, with the rate of change depending on the foulant thickness and a dimensionless (adjustable) constant $k_a$. A suitable choice of $k_a$ allows defining faster or slower evolution of the roughness to its final value.

These conceptual models are used here in the absence of reliable, dynamic data and a mechanistic model. The results do, nevertheless, highlight the importance of including a suitable roughness model.

### *Initial and boundary conditions*

At all points $z$ along the axis, at time $t = 0$:

1) The tube is clean (i.e., no fouling layer)

$$R_f(z) = 0; \quad \forall z \tag{32}$$

2) The thickness of fouling layer, $\delta$, is initialized to a small positive value ($10^{-7}$ m, with associated surface roughness $e^0$) for numerical reasons

$$\delta(z) = 10^{-7}; \quad \forall z \tag{33}$$

3) The temperature profiles at time 0 are assumed to be in steady in all domains

$$\frac{dT_w(z,r)}{dt} = \frac{dT_l(z,r)}{dt} = \frac{dT(z)}{dt} = 0, \quad \forall(z,r) \tag{34}$$

4) The aging model given by Eq. 18 introduces a differential equation which needs an initial value of the youth variable

$$y(z,r) = 1; \quad \forall(z,r) \tag{35}$$

Two typical operating conditions are considered: uniform heat flux (UHF), and uniform wall temperature (UWT). In both cases shell-side effects are ignored, and represented by the boundary conditions on the outside of the tube wall (at $r = R_o$).The UHF case corresponds to the tube being heated through the wall (for example, by an electric cartridge heater), with a fixed value of the heat flux at the outer tube surface, $q_o$. The boundary condition, is, therefore

$$q_w(z,R_o) = q_o \tag{36}$$

In the UWT case the temperature of the tube outer surface is fixed at $T_o$ for all times and axial values

$$T_w(z,R_o) = T_o \tag{37}$$

In both the aforementioned cases, the following boundary conditions apply at the interface with the other domains. At the interface between $\Omega_w$ and the fouling layer $\Omega_l$, there is continuity in the heat flux and the temperature at all times

$$q_w(z,R_i) = q_l(z,R_i) \tag{38}$$

$$T_w(z,R_i) = T_l(z,R_i) \tag{39}$$

Or, for dimensionless domain $\tilde{\Omega}_l$

$$q_w(z,R_i) = q_l(z,0) \tag{40}$$

$$T_w(z,R_i) = T_l(z,1) \tag{41}$$

At the moving boundary between the fouling layer $\Omega_l$, and the tube-side domain $\Omega_t$ there is continuity in the heat flux

$$q_l(z,R_{flow}) = -h_t(T_l(z,R_{flow}) - T(z)) \tag{42}$$

Or, for dimensionless domain $\tilde{\Omega}_l$

$$q_1(z,1) = -h_t(T_l(z,1) - T(z)) \tag{43}$$

At the tube inlet (all $t$, $r$) the oil temperature $T_{\text{in}}(t)$, and pressure $P_{\text{in}}$ $(t)$ are supplied functions of time

$$\begin{aligned} T(0) &= T_{in} \\ P(0) &= P_{in} \end{aligned} \tag{44}$$

### *Solution method*

The model outlined in the previous section consists in a set of partial differential and algebraic equations. All equations were modeled and solved using the gPROMS™ modeling environment.[36] The partial differential equations are solved using a second-order centered finite difference method with all domains discretized in 10 points in the axial direction.

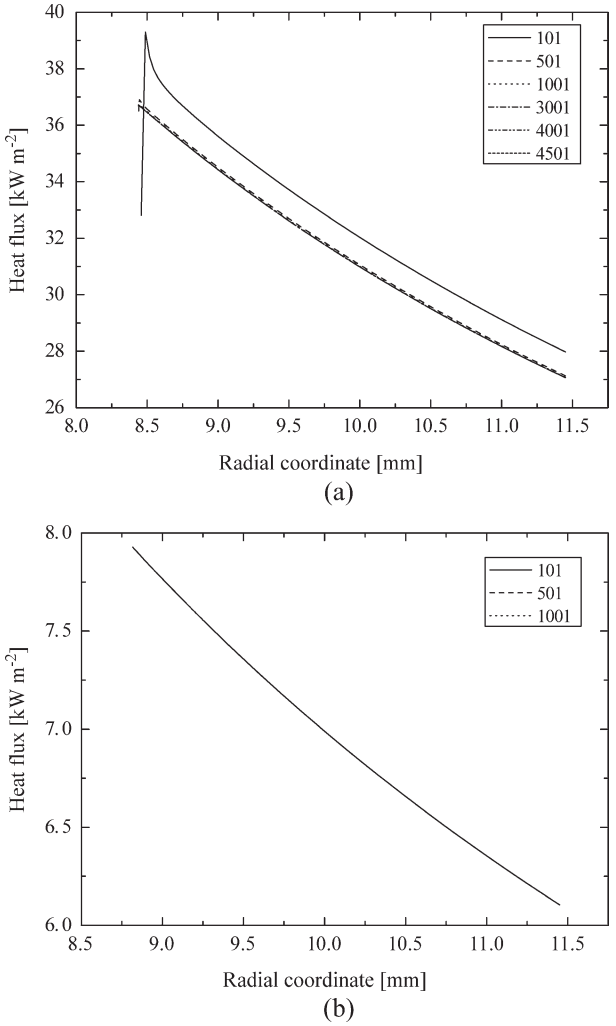


**Figure 4. Mesh independency test.**

Radial heat flux after a year in case of (a) fast and (b) intermediate ageing. The legend indicates the number of discretisation points used in simulations. The fact that curves overlap confirms that no additional accuracy is obtained with more points.

While solution for no aging and slow aging conditions does not present substantial challenges for the numerical solver, calculations for the constant heat flux cases at fast aging conditions proved to be more critical. The reason is that fast aging produces steep profiles of the thermal conductivity in the radial direction (as reported in the results section) in regions close to the interface between domains $\Omega_l$ and $\Omega_t$. To ensure accuracy of the solution a mesh independency test was performed for the most challenging conditions (combination of fast aging and fast fouling rates). Figure 4a reports the results of this test, showing that satisfactory accuracy is achieved with 3001 or more discretization points. Figure 4b shows the absence of numerical problems when integrating under slow aging conditions. 3001 points, were, therefore, used in the radial direction for the $\Omega_l$ domain, whereas 10 points were considered sufficient for the $\Omega_w$ domain.

**Table 3. Summary of Fouling, Aging Model Parameters**

| Parameter | Symbol | Units | Value |
|---|---|---|---|
| Fouling activation energy | $E_f$ | kJ mol$^{-1}$ | 28 |
| Fouling deposition constant | $\alpha$ | m$^2$K kW$^{-1}$ h$^{-1}$ | 4100 |
| Fouling suppression constant | $\gamma$ | m$^2$K kW$^{-1}$ h$^{-1}$Pa$^{-1}$ | $2.63 \times 10^{-5}$ |
| Slow ageing pre–exponential factor | $A_s$ | s$^{-1}$ | $10^{-4}$ |
| Intermediate ageing pre–exponential factor | $A_i$ | s$^{-1}$ | $10^{-3}$ |
| Fast ageing pre–exponential factor | $A_f$ | s$^{-1}$ | $10^{-2}$ |
| Ageing activation energy | $E_a$ | kJ mol$^{-1}$ | 50 |

## Application

The geometric and physical property parameters for a base case representing a tube in an oil refinery exchanger are reported in Table 2. The fouling rate parameters in Table 3 were selected as being representative of typical refinery heat exchangers.[11] The aging model activation energy $E_a$, was fixed at a realistic, but nevertheless assumed, value of 50 kJ mol$^{-1}$. It should be noted that both the form of the fouling model (Equation 24), and the values used for the aging model parameters differ from those employed by Ishiyama et al.[9] The fouling and aging models are, in fact, independent and the latter can be applied to different fouling mechanisms as long as the evolution in thermal conductivity can be satisfactorily described by first-order kinetics. In this article, fouling rates are larger than those studied by Ishiyama et al.[9] resulting in larger thicknesses of fouling layers in the cases studied.

The fluid properties used (Table 2) are representative of typical crude oils. The inlet oil temperature and pressure were kept constant at the values indicated in Table 2.

In the following sections, the aforementioned model is used to study the effect of roughness dynamics (*Impact of surface roughness dynamics* section), and the impact of deposit aging (*Impact of aging* section) on heat transfer. Different time scales of investigation are considered in the two cases to reflect experimental evidence. Increase in roughness due to fouling affects the overall heat-transfer coefficient within hours,[18] whereas aging is expected to manifest its effects over days or months of operation.[9]

### *Impact of surface roughness dynamics*

The effect of surface roughness on the initial stages of fouling was explored in the absence of deposit aging (by setting $A_a$ to 0 s$^{-1}$) to decouple the two effects. The timeframe used is 80 h of operation, starting from an initially clean tube surface. Roughness is expected to give rise to measurements of negative fouling resistance, as reported experimentally by Knudsen et al.[18] in the first 50 h of operation. Over this relatively short time scale the operating mode does not have a great influence on deposition, and so only the UWT case was investigated, with Eq. 37 as the boundary condition at the tube outer wall. The linear and asymptotic models proposed to capture the roughness dynamics are investigated with particular reference to the impact of deposit roughness on overall heat-transfer coefficient, and, thereby, fouling resistance.

The parameter $k_p$ in the linear model (Eq. 29) was arbitrarily fixed to 4, so that the time scale in which a negative fouling resistance is predicted by the model is within that experimentally observed by Knudsen et al.[18] Simulations for other values of this parameter can be easily performed, as required. Figure 5 shows the variation of roughness over time in a section in the middle of the tube (i.e., $z = L/2 =$ 3 m) for the linear model. At the deposition rate achieved in this case (to which the roughness is related) the final roughness value of 150 $\mu$m is reached after ca. 70 h of operation. Figure 5b shows the evolution of roughness at the same location given by the asymptotic model (Eq. 31) for different values of the constant $k_a$, compared to the no fouling case. Depending on the value set for the $k_a$ parameter, the time at which the asymptotic value of roughness is reached changes.

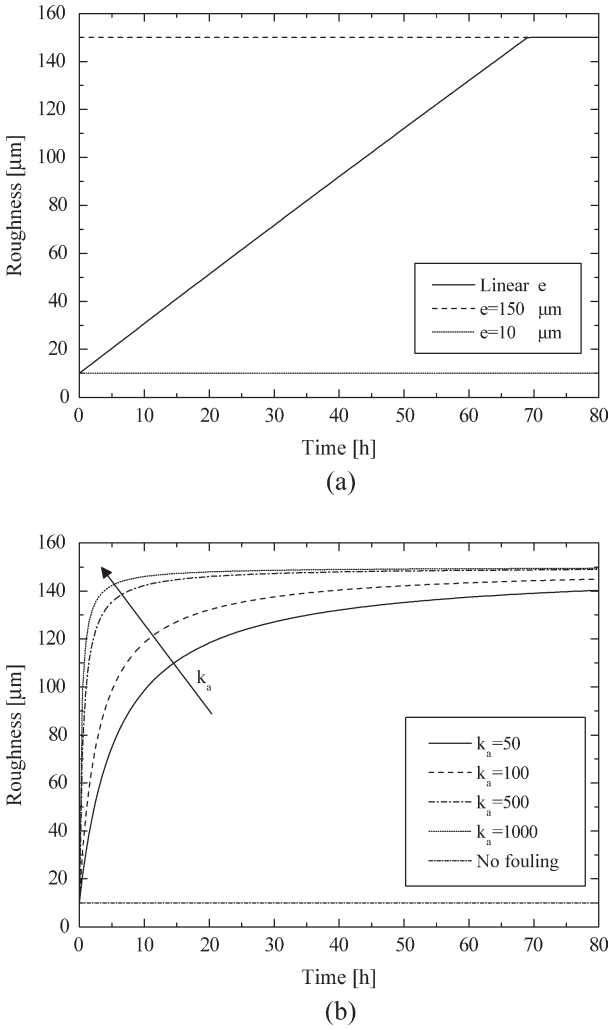


**Figure 5. Evolution of roughness at the tube midpoint ($z = L/2$) as a function of time for (a) linear (Eq. 29), and (b) asymptotic (Eq. 31) models with different values of the constant $k_a$ compared to the no-fouling case.**

When no fouling occurs, the roughness value remains at that of the clean tube $e^0$, i.e., 10 $\mu$m.

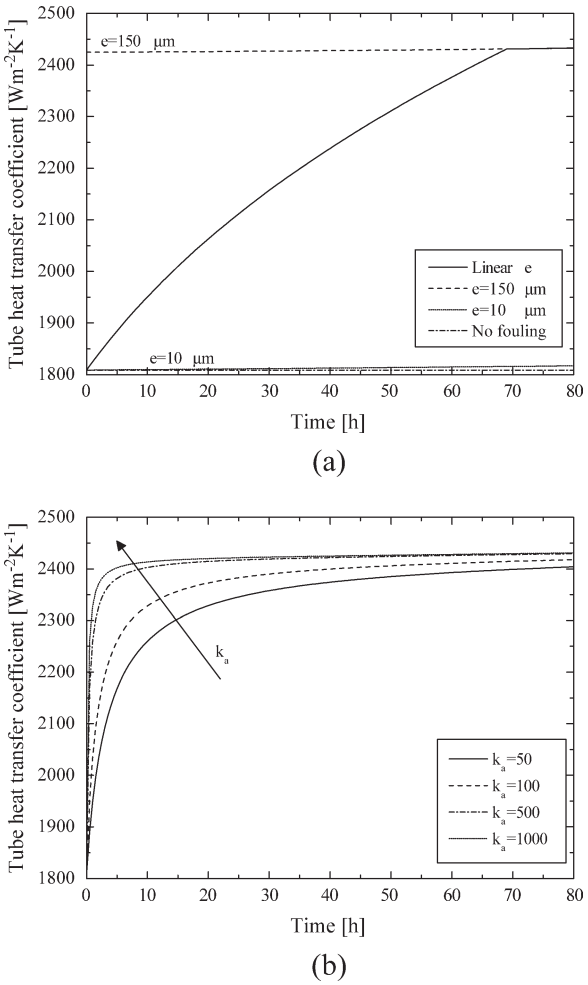


**Figure 6. Effect of roughness evolution on the tube film heat-transfer coefficient (a) linear, and (b) asymptotic models with different values of the parameter $k_a$.**

Figure 6a also shows the effect of deposit layer growth without any change in roughness (solid line, $e = 10$ $\mu$m).

For $k_a = 1{,}000$, 15 h are sufficient to reach the 150 $\mu$m considered as maximum roughness, whereas for smaller values of the same parameter ($k_a = 50$ and $k_a = 100$), more than 80 h are needed. Due to the short time horizon, there is no significant difference in thickness along the length of the tube (only 1 $\mu$m after a year of operation). However, it becomes much larger inside the tubes for longer periods (see later Figure 12).

Figure 6a shows how the increase of surface roughness affects the tube-side convective heat-transfer coefficient $h_t$. For comparison, the plot also shows the results for cases with constant roughness (at $e^0$ and $e^\infty$), and with no fouling. In the no-fouling case, there are no variations in cross-sectional area or roughness to affect the heat-transfer coefficient, which, therefore, remains constant at the clean tube value, over the whole time horizon. With deposition and constant roughness, the reduction in cross-sectional area in both cases considered increases the oil velocity, giving a small rise to $h_t$ (barely noticeable in Figure 6a by comparison with the no-fouling case). A linear variation in roughness, on the other hand, produces a large increase in the film convective heat-transfer coefficient, from a clean tube value of 1,800 W m$^{-2}$ K$^{-1}$ to about 2,400 W m$^{-2}$ K$^{-1}$ after 70 h, when the final deposit roughness of 150 $\mu$m is reached. When the asymptotic roughness model is used (Figure 6b), the increase in convective heat transfer is more rapid, depending on the value for the parameter $k_a$ used. With both models, the value of $h_t$ obtained after a few hours with a rough deposit is substantially (i.e., 1/3) higher than in a clean tube.

The increase in convective heat-transfer coefficient is evident in the plot of the overall thermal resistance (Figure 7), calculated as the inverse of the overall heat-transfer coefficient in Eq. 27. In case of constant fouling roughness (Figure 7a), set at a minimum value of $e = 10$ $\mu$m, a linear increase in the overall thermal resistance, from the no-fouling value (horizontal dashed-dotted line) is seen. The same linear behavior is exhibited by the system for a constant $e = 150$ $\mu$m; however, the clean surface heat-transfer resistance (at time zero) is smaller (0.0010 m$^2$ W$^{-1}$ K$^{-1}$), owing to the

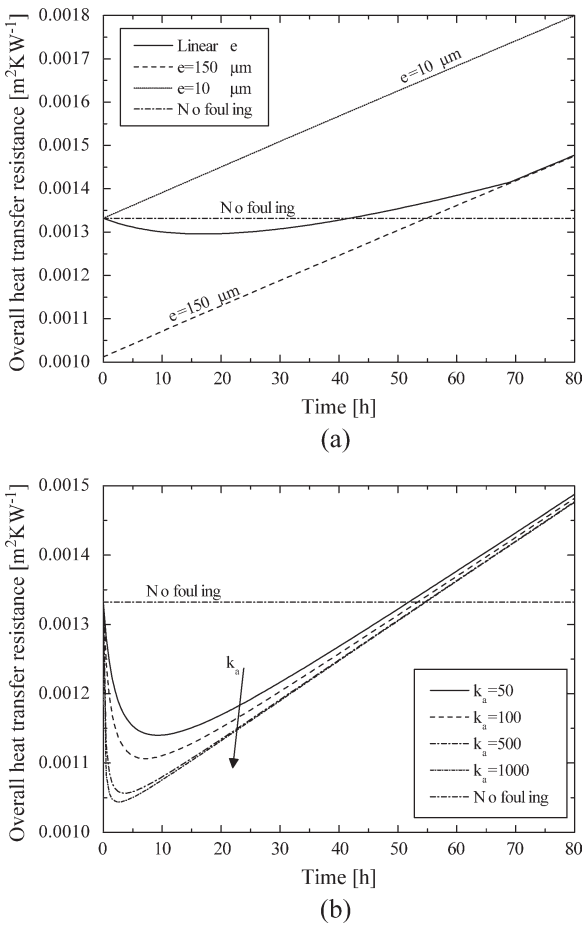


**Figure 7. Overall heat-transfer resistance for (a) linear, and (b) asymptotic roughness models with different values of the constant $k_a$ compared to the no-fouling case.**

Plot (a) also shows the result obtained for deposit growth with no change in roughness.

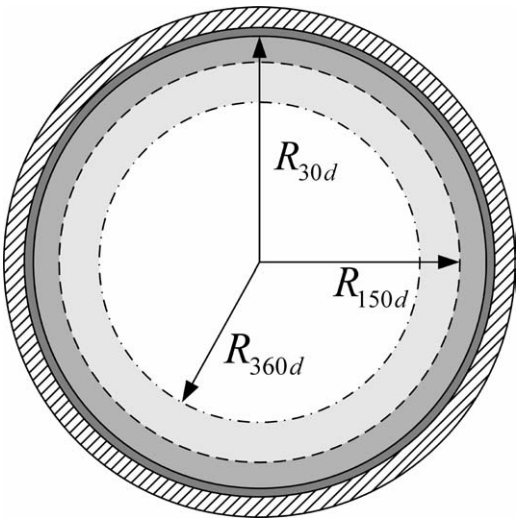


**Figure 8. Graphical representation of fouling layer thickness after 10, 150 and 360 days for the case of UHF and fast aging.**

After a year of operation, the cross-sectional area available for the fluid flow is reduced by ca. 50%.

larger contribution to the convective heat transfer from a rougher surface. The linear roughness model (continuous line in Figure 7a) produces an initial decline in the overall thermal resistance below that of no-fouling conditions over the first 17 h of operation. At this time, the heat-transfer enhancement given by the increase in roughness balances the decrease in heat transfer given by fouling deposition, i.e., the sum of the two following contributions is zero

$$\frac{d}{dt}\left(\frac{1}{\bar{h}_t}\right)+\frac{d\bar{R}_f}{dt}=0 \tag{45}$$

At this time, the thickness of the fouling layer is 8.9 $\mu$m. Thereafter, the increase in the deposit layer resistance becomes larger, but the overall resistance is still smaller than the no-fouling value, which is reached after 40 h, when the thickness of the fouling layer is 20.6 $\mu$m. Figure 7b shows the results obtained with the asymptotic roughness model. A strong decline in heat-transfer resistance is observed over the first 10 h of operation for small values of parameter $k_a$, whereas it is limited to the first 5 h for larger values ($k_a$ = 500). In the case of $k_a$ = 1,000, the two contributions in Eq. 45 counterbalance after 2.5 h, when the thickness of the fouling layer is only 1.4 $\mu$m. In all cases, the overall heat-transfer resistance is below the no-fouling value for up to 52–55 h.

### *Impact of aging*

Here we wish to investigate the impact of aging on fouling, and, hence, thermal and hydraulic performance of the exchanger tubes. Unlike deposit roughness, these effects

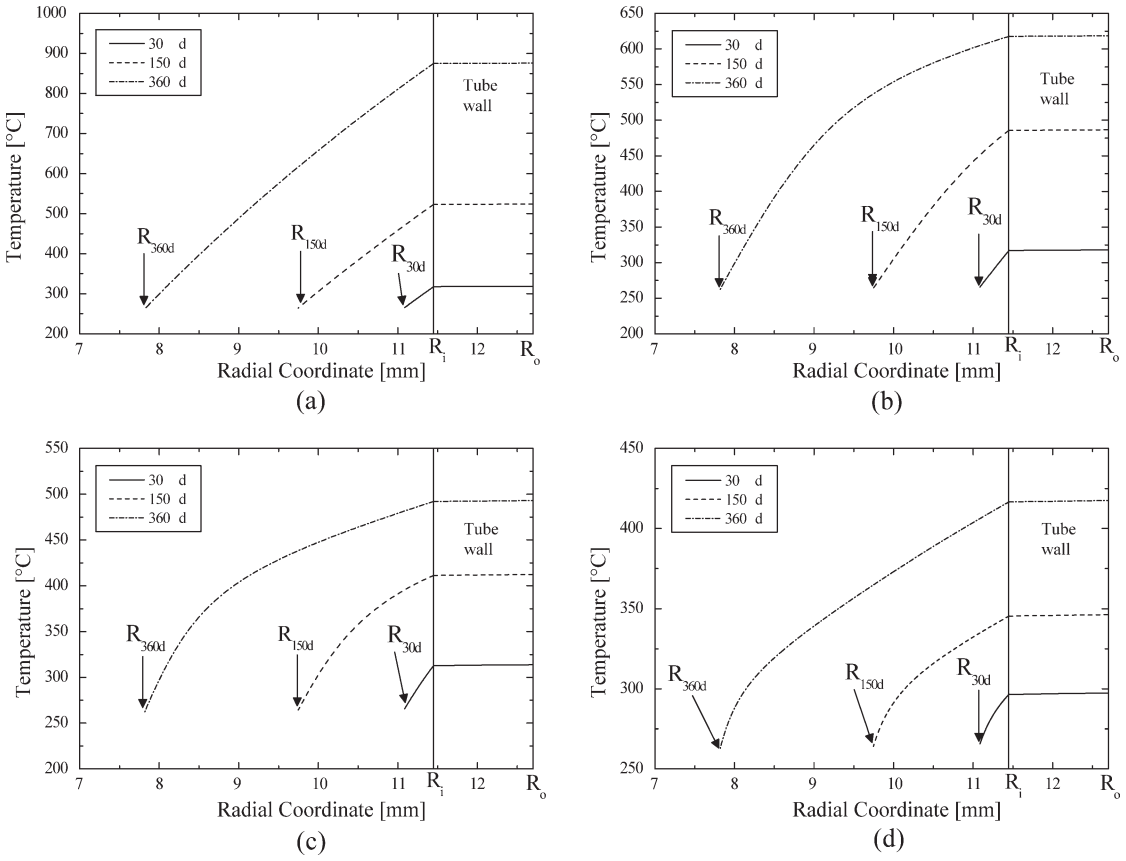


**Figure 9. Radial temperature profiles for uniform heat flux operation for a section at the tube midpoint in the case of (a) no-aging, (b) slow, (c) intermediate, and (d) fast aging.**

The vertical dotted line indicates the location of the tube wall $R_i$.

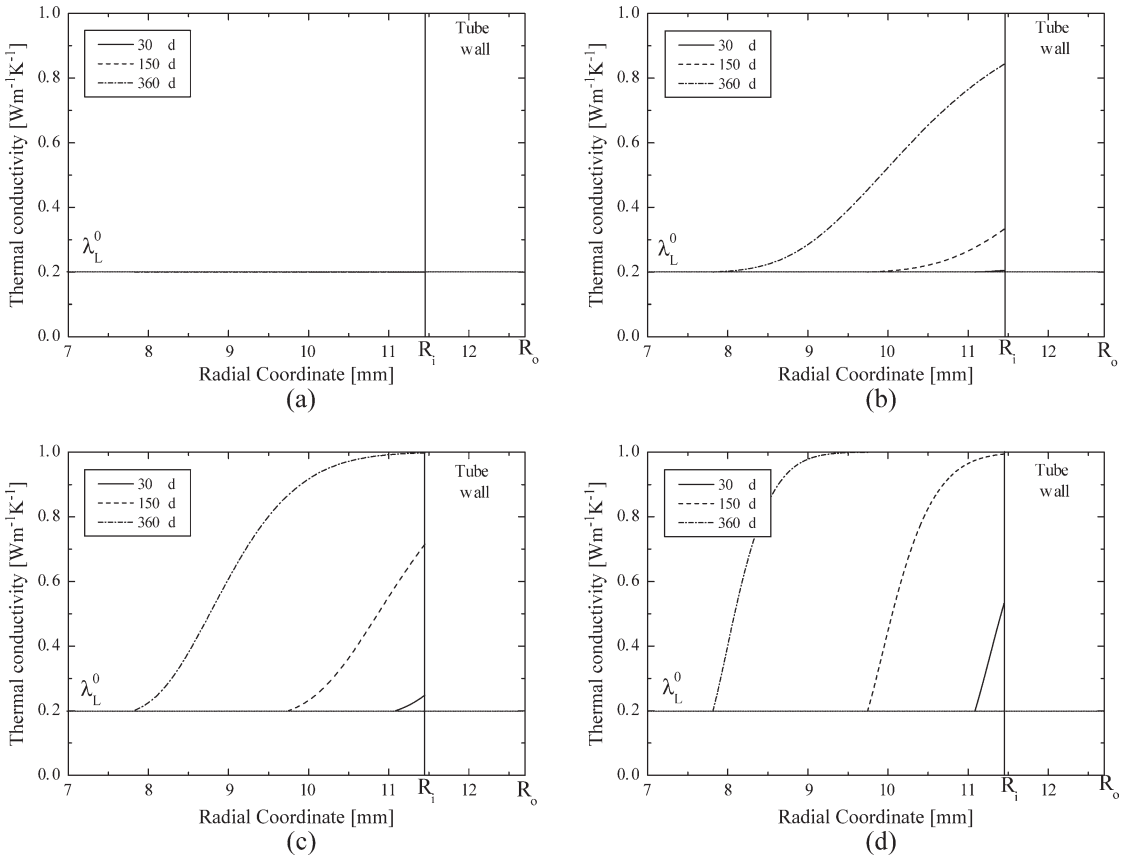


**Figure 10. Deposit thermal conductivity distribution for uniform heat flux operation for a section at the tube midpoint in the case of (a) no-aging, (b) slow aging, (c) intermediate, and (d) fast aging.**

typically impact medium and long-term operation (timescales of weeks to months). We also wish to demonstrate the benefits of a distributed model.

It should be noted that, presently, due to a lack of detailed experimental data, the values of the parameters for the aging kinetic model cannot be estimated. A parametric study showing the relative importance of the pre-exponential factor $A_a$, and the activation energy $E_a$, in Eq. 18 was proposed in Ishiyama et al.[9] based on realistic estimates of the aging parameters. In this work, the activation energy of the aging reaction $E_a$, was set at 50 kJ/mol. The aging speed is governed by the values of the pre-exponential factor $A_a$, and three cases were considered corresponding to "fast aging" ($A_f = 10^{-2}$ s$^{-1}$), "intermediate aging" ($A_i = 10^{-3}$ s$^{-1}$) and "slow aging" ($A_s = 10^{-4}$ s$^{-1}$). Values for this parameter were set arbitrarily, based on previous simulations.[9]

The results in the following sections are reported for the two operating modes discussed earlier:

1) Uniform heat flux (UHF). For comparison, the value of the heat flux in this case was selected to give the same initial wall outer temperature as in the following UWT mode;

2) uniform wall temperature (UWT), with an outer wall temperature of 270°C.

In both cases, the mass flow rate was fixed at 0.3 kg s$^{-1}$. The reduction in cross-sectional area caused by fouling is accompanied by an increase in pressure drop which must be compensated for by increasing pumping power. An alternative scenario, of constant pressure drop (i.e., mass flow rate decreasing over time), was explored by Ishiyama et al.[9] and is not repeated here. The inlet oil temperature was constant, at 250°C, in both cases.

### *Uniform heat flux (UHF) operation*

In this case, the deposition rate is almost constant, and the time transform in Eq. 15 holds good.

The effects of aging can be appraised by considering the temperature and thermal conductivity profiles within the deposit at different times. Figure 8 depicts, graphically, the thickness of the fouling layer in the case of fast aging at three different times, namely after 30, 150 and 360 days of operation. The flow radius $R_{\text{flow}}$ defined in Eq. 5 at each instant is termed as $R_{30d}$, $R_{150d}$, $R_{365d}$, respectively. The sizeable reduction in duct flow diameter (30%, ca. 50% in cross-sectional area) after one year is evident.

Radial temperature profiles across the tube wall and the fouling layer located at the middle of the tube (i.e., $z = L/2 = 3$ m), at the aforementioned times, are reported in Figure 9, for the four cases of (a) no aging, (b) slow, (c) intermediate, and (d) fast aging. For consistency in the comparison with the next operating mode, the value for the heat flux fixed at the boundary is the same as the initial value at midpoint section of the tube in the UWT case. It is clear that to sustain the required rate of heat transfer the temperature at the wall has to increase. With no aging (Figure 9a), and slow aging (Figure 9b), the high-thermal resistance given by

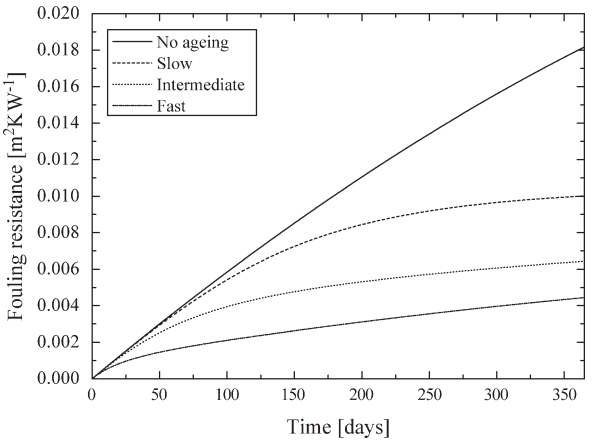


**Figure 11. Uniform heat flux operation: aggregate fouling resistance over time for different aging speed as calculated via Eq. 26.**

a low-conductivity layer results in a large increase in this wall temperature (above 500°C after six months). Unrealistic values would clearly be reached over this and longer time scales. With intermediate and fast aging (Figure 9c and d), for these operating parameters, the wall temperature remains below 450°C owing to the higher thermal conductivity of the aged deposit, which in turn reduces the impact of fouling on the overall heat-transfer coefficient. Similar profiles were observed at other locations along the tube.

The consequence of UHF operation is that the surface temperature increases as fouling progresses, whereas with UWT operation the temperatures decrease. As a result, UHF operation causes a large change in thermal conductivity, even at the low-aging speed (Figure 10b). The asymptotic value of $\lambda_l^{\infty}$ is not reached after one year, but over half of the layer has doubled its thermal conductivity by this time. The limiting value $\lambda_l^{\infty}$, is reached both with intermediate and fast aging speeds (Figure 10b and c). In particular, the combination of high-temperature and fast aging results in zones of steep change in thermal conductivity in the foulant layer close to the interface with the crude flow. In the limiting case, aging would occur instantaneously.

In order to relate these results to current practice, it is useful to aggregate the distributed values into the customary measure of fouling, the overall fouling resistance. The effect of aging on the average fouling resistance, (calculated via Eq. 26) is presented in Figure 11. The higher the aging rate, the lower the fouling resistance, as expected. The important result, that this thermal measure of fouling does not give an accurate representation of the deposit layer thickness (and associated pressure drops), is evident.

The small deviation from linearity of the fouling profile for the no-aging case shown in Figure 11 is due to the significant change in cross-sectional area available for flow caused by the high-deposition rate (i.e., the parameters used in the fouling model). Curvature affects the estimation of thermal resistance, but the main factor is the change in the suppression contribution to the deposition rate (Eq. 24) causing the deposition rate to change from its initial value.

### *Uniform wall-temperature (UWT) operation*

In this case, the deposition rate is expected to change owing to the change in deposit/liquid interface temperature. However, as noted in previous sections, when the deposition rate is not linear, Eq. 15 represents a conservative estimate of the age of each element. The error introduced can be estimated by comparing, through simulations, the actual thickness with that obtained if the deposition rate throughout the operation was constant, at the initial values. As the fouling rate is temperature-dependent, the assumption of linearity is least accurate for the case of constant wall temperature with slow aging, where the surface temperature will change noticeably with time. In this particular case, the difference in thickness between the linear and the nonlinear deposit-time profiles was not considered to be significant (less that 1% difference) over the first 80 days of operation, whereas the deviation reaches ~19% after a year of operation. We acknowledge this limitation in the aging time transformation: this is the subject of ongoing work.

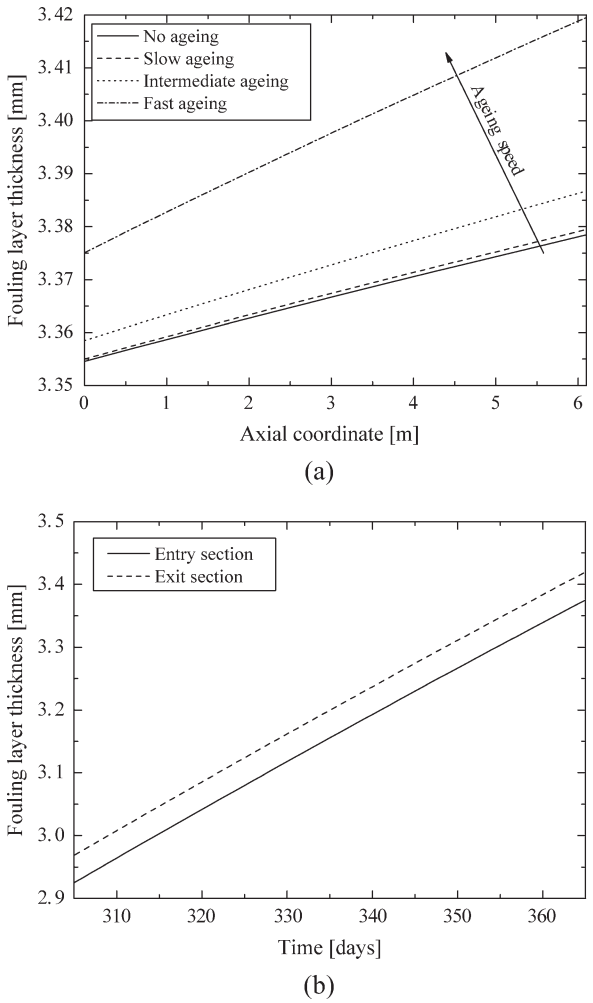


**Figure 12. Fouling layer thickness along the tube, uniform wall temperature mode: (a) after a year of operation, for different aging speeds, and plot (b) shows the fouling layer thickness at the tube entry and exit over the last 60 days of operation for the fast aging case.**

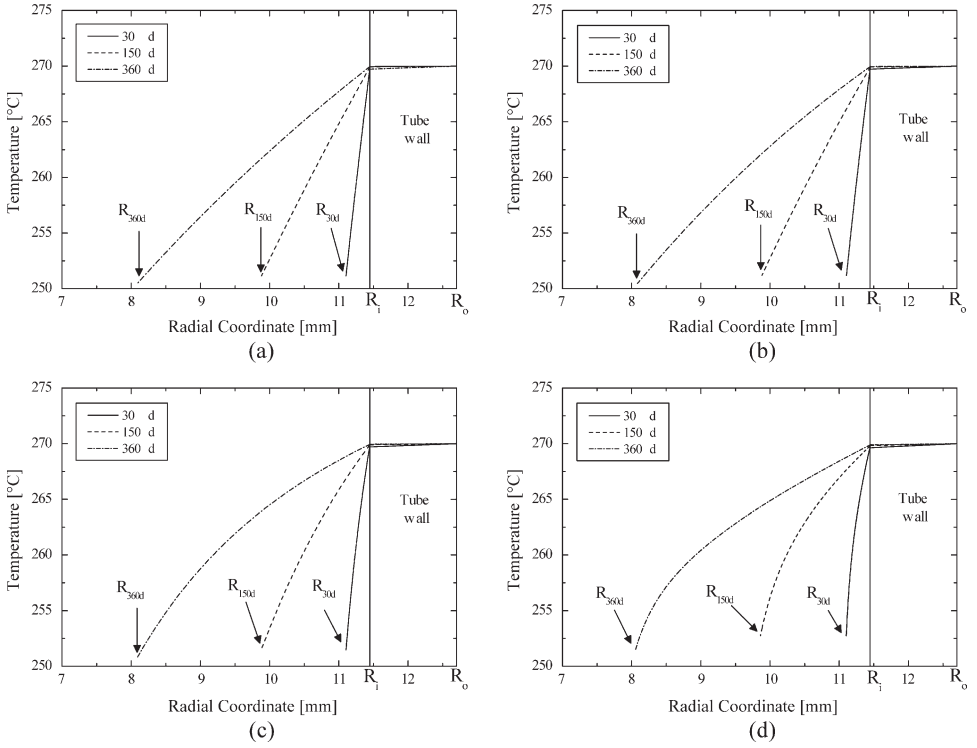


**Figure 13. Radial temperature profiles obtained for uniform wall temperature operation across a section at the tube midpoint in the case of (a) no-aging, (b) slow, (c) intermediate, and (d) fast aging.**

The vertical solid line indicates the location of the tube wall $R_i$.

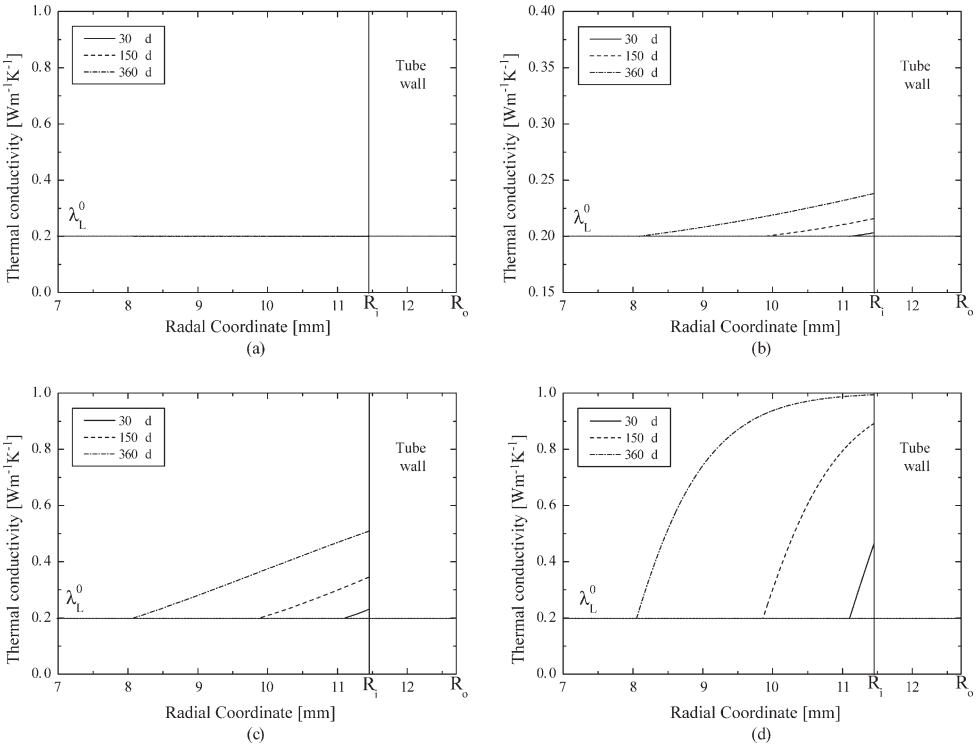


**Figure 14. Evolution of deposit thermal conductivity for uniform wall temperature operation for a section at the tube midpoint in the case of (a) no-aging, (b) slow, (c) intermediate, and (d) fast aging.**

The distributed model is able to incorporate the effects of changing temperature conditions across the tube. Figure 12 shows how the aging speed affects the fouling layer thickness along the length of the tube after one year of operation. The faster the aging, the larger is the portion of the fouling layer which, at a given time, has changed to a higher thermal conductivity form. This results in higher-temperatures within and across the deposit, which in turn promotes deposition and yields larger layer thicknesses. At the exit of the tube, there is a 40 $\mu$m difference between the no-aging and fast aging cases.

Figure 12b shows the deposit thickness at the entry and exit sections of the tube over the last 60 days of simulated operation for the fast aging case (i.e., the worst case). The deposit thickness is greater at the exit, owing to the higher fluid-deposit interface temperature at this location. The difference is not large, mainly because the change in temperatures across the tube considered here is quite modest: much larger temperature changes can occur in operating units and the model can handle these readily.

Figure 13 shows radial temperature profiles in the tube wall and the fouling layer at the midpoint of the tube (i.e., $z = L/2 = 3$ m), after 30, 150 and 360 days of operation in UWT mode for the four cases of (a) no aging, (b) slow, (c) intermediate, and (d) fast aging. After a year of operation, in all cases considered, there is a significant drop in temperature at the interface between the fouling layer and the flowing liquid. In the case of no-aging (Figure 13a), and slow aging (Figure 13b), the temperature profile shows a similar, linear trend. However, with intermediate and fast aging (Figure 13c and d), the temperature profiles are no longer linear as a result of the changing thermal conductivity in the radial direction (see Figure 14). Most of the heat-transfer resistance is developed across the younger, lower conductivity deposit layers located near the deposit/fluid interface. The layer-liquid interface temperatures at any one time in the four cases (a) to (d) are increasingly different, although this may not be so apparent from Figure 13 even after 360 days, due to the scales used in the graph. This is more clearly reflected in the tube exit temperature profiles, shown later in Figure 16.

In the no-aging case the thermal conductivity is, by definition, constant, at the initial value $\lambda_l^0$, throughout the time horizon (Figure 14a). Aging causes an increase in thermal conductivity at coordinates close to the tube metal wall as a consequence of the combined effect of age (residence time) and high-temperature. In the case of slow aging (Figure 14b), this increase is modest (ca. 20%) compared to that in case of intermediate aging in Figure 14c (ca. 150%). Both cases show a linear variation of $\lambda_l$ along the radial coordinate and the final value of thermal conductivity typical of coke deposits,, is not reached over this time scale. With fast aging (Figure 14d, the profile is no longer linear, and after six months of operation a five-fold increase in $\lambda_l$ (from $\lambda_l^0$ to $\lambda_l^\infty$) is reached in regions close to the tube wall. With time, other sections along the radial coordinate increase their thermal conductivity, approaching the asymptotic value $\lambda_l^\infty$. After a year of operation, ca. 8% of the deposit layer has a thermal conductivity above 0.99 W m$^{-1}$ K$^{-1}$, indicating an almost complete change to "coke" in that section.

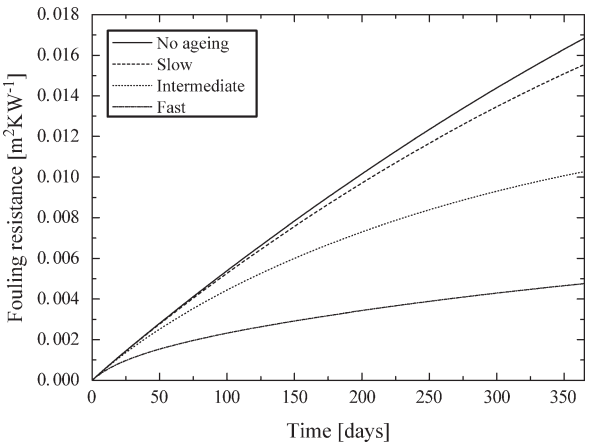


**Figure 15. Aggregate fouling resistance (evaluated using Eq. 26) over time for different aging speeds, uniform wall temperature.**

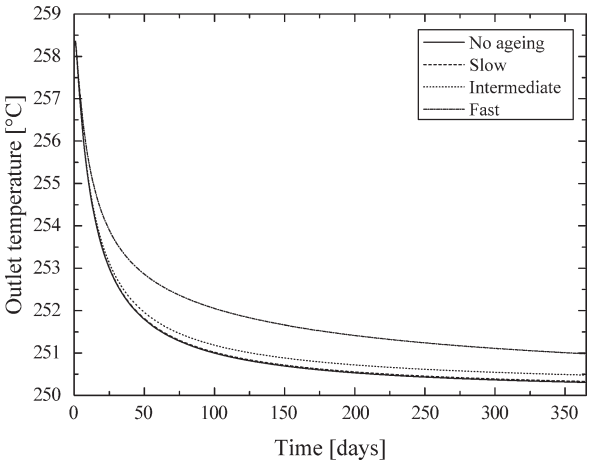


**Figure 16. Effect of aging speed on crude oil outlet temperature, uniform wall temperature scenario.**

For comparison with the previous UHF case, Figure 15 reports the average fouling resistance $\overline{R}_f$ (calculated via Eq. 26). The trend shown with the changing speed of aging is the same as the UHF case (Figure 11); however, a larger deviation with respect to the no-aging case is seen in the latter case which further highlights the importance of considering aging in accelerated fouling tests.

At a macroscopic level, a beneficial effect of aging can be observed on the oil temperature at the tube outlet (Figure 16). The increase in thermal conductivity given by fast aging (as reflected by the fouling resistance in Figure 15) produces a slower decline in outlet temperature compared to the case with slower or no aging. This difference in outlet temperature results in a significant difference between the fouling Biot number $Bi_f$ ( $= \overline{R}_f \overline{h}_t$), in the different cases considered. After a year of operation, in fact, $Bi_f$ for the no aging case is ca. 86, whereas it is ca. 40% less in the case of fast aging ($Bi_f = 52$).

## Conclusions

A distributed model for a single tube undergoing crude oil fouling has been developed. This uses a novel way of modeling the continuous growth of deposit distributed over time

and space, via a moving boundary formulation developed by Coletti and Macchietto[24] which provides a sound and general formulation as a set of partial differential and algebraic equations in cylindrical coordinates. In this article, first a suitable transformation in the time domain allowed incorporating the aging model of Ishiyama et al.[9] It has been shown that this approach is rigorously valid for the special case of linear deposition, whereas it represents a reasonable approximation in other cases. However, several assumptions previously introduced were relaxed: (1) the underlying fouling model now includes a suppression term (the Ebert-Panchal model was used here, but in principle other deposition-suppression models could be used); (2) the use of circular coordinates overcomes the need for a ''thin-slab'' assumption and allows modeling large deposits relative to tube diameter, and (3) a local aging history can be calculated for each point along the length of the deposit, rather than an overall, ''lumped'' value for averaged conditions. In addition, the assumption of constant deposit roughness was relaxed with the use of two novel models proposed to capture the effects of deposition on roughness and heat transfer. While the underlying physics of the evolution of roughness is unknown, the models represent plausible approximations.

Simulations were performed for two typical operating modes (UWT and UHF). Geometry, flow rate (fixed to a constant value) and fouling behavior used in the studies presented are typical of oil refineries. The results, extending the previous model's findings, highlight the importance of considering deposit formation and aging in industrial applications where the time scale is of weeks to several months. They show that even for the case considered as slow aging the impact on the fouling resistance is significant. Accounting for roughness dynamics, on the other hand is important to aid interpretation of short time scale pilot scale tests.

The results show that the roughness model can explain some otherwise puzzling phenomena such as (apparent) initial negative fouling resistance that cannot be captured otherwise. Overall, the model and results enable capturing and improving our understanding of the complex interaction between thermal, hydraulic and aging effects in a fouling heat exchanger tube. The results presented are clearly applicable to other geometries (annular tubes) and full-scale equipment (multipass heat exchangers). Validation of various model components (e.g., surface roughness) and estimation of parameters for others (e.g., aging) will require quality experimental data. A research program to provide them is under way (Macchietto et al.[37]).

## Acknowledgments

Funding from EPSRC projects EP/D50306X/1 and EP/D503051/1, as well as financial support for EMI from the Cambridge Overseas Trust is gratefully acknowledged.

## Notation

$A$ = area $m^2$
$A_a$ = frequency factor of the aging model $s^{-1}$
$A_{flow}$ = cross-sectional area for flow, $m^2$
$A_m$ = logarithmic mean area, $m^2$
$c_p$ = specific heat at constant pressure, J $kg^{-1}$ $K^{-1}$
$C_f$ = fanning friction factor
$d$ = diameter, m
$E$ = activation energy, J $mol^{-1}$
$e$ = tube surface roughness, m
$F$ = heat exchanger configuration correction factor
$h_t$ = convective film heat-transfer coefficient, W $m^{-2}$ $K^{-1}$
$\bar{h}_t$ = average convective heat-transfer coefficient, W $m^{-2}$ $K^{-1}$
$k_a$, $k_p$ = roughness model parameters
$k_t$, = roughness model parameter, s
$L$ = length
$\dot{m}$ = mass flow rate, kg/s
$Nu$ = Nusselt number
$P$ = pressure, Pa
$Pr$ = Prandtl number
$Q$ = heat duty, W
$q$ = heat flux, W $m^{-2}$
$q_0$ = heat flux at the tube outer wall, W $m^{-2}$
$Re$ = Reynolds number
$R$ = radius, m
$R_f$ = fouling thermal resistance, $m^2$ K $W^{-1}$
$\bar{R}_f$ = aggregated fouling thermal resistance, $m^2$ K $W^{-1}$
$R_{flow}$ = flow radius, m
$R_g$ = universal gas constant J $kg^{-1}$ $mol^{-1}$
$r$ = radial coordinate, m
$\tilde{r}$ = dimensionless radial
$T$ = temperature, K
$T_f$ = film temperature, K
$t$ = time, s
$t_{age}$ = aging time, s
$U$ = overall heat-transfer coefficient, W $m^{-2}$ $K^{-1}$
$U_{clean}$ = overall heat-transfer coefficient in clean conditions, W $m^{-2}$ $K^{-1}$
$u$ = mean fluid velocity in the tube, m $s^{-1}$
$y$ = youth variable
$z$ = axial coordinate, m

### Subscripts

$a$ = aging
$b$ = bulk
$l$ = fouling layer
$f$ = fouling, fast aging
$i$ = inner, intermediate aging
$in$ = inlet
$o$ = outer
$s$ = slow aging
$t$ = tube-side
$w$ = wall

### Superscript

$0$ = initial state
$\infty$ = final state

### Greek letters

$\alpha$ = deposition constant, $m^2$ K $kW^{-1}$ $h^{-1}$
$\Delta T_{lm}$ = logarithmic mean temperature difference, K
$\delta$ = foulant thickness, m
$\theta$ = angular coordinate, rad
$\lambda$ = thermal conductivity, W $m^{-1}$ $K^{-1}$
$\mu$ = dynamic viscosity, Pa s
$\nu$ = kinematic viscosity, $m^2$ $S^{-1}$
$\nu_0$ = kinematic viscosity at 100°F $m^2$ $s^{-1}$
$\rho$ = density, kg $m^{-3}$
$\gamma$ = suppression constant, $m^2$ K $kW^{-1}$ $h^{-1}$ $Pa^{-1}$
$\tau$ = wall-shear stress, Pa
$\Omega$ = model domain
$\tilde{\Omega}$ = dimensionless model domain

## Literature Cited

1. Müller-Steinhagen H. Fouling of heat exchangers surfaces. *Chem Ind*. 1995;5:171–175.
2. Bott TR. Fouling of heat exchangers. *Fuel Energy Abstracts*. 1996; 37:211–211.
3. Thackery PA. The cost of fouling in heat exchanger plant. In: *Fouling: Science or Art?, Inst Corrosion Sci & Tech and Inst Chem Eng*: University of Surrey, Guildford, U.K; 1979.

4. Van Nostrand WL, Leach SH, Haluska JL. Economic Penalties Associated with the Fouling of Refinery Heat Transfer Equipment. In: Somerscales EFC, Knudsen JG, eds. *Fouling of Heat Transfer Equipment*. Troy, New York: Hemisphere; 1981;619–643:13–17.
5. Epstein N. Thinking about heat transfer fouling: a 5 × 5 matrix. *Heat Transfer Eng*. 1983;4:43–56.
6. Nelson WL. Fouling of heat exchangers. *Refin Nat Gas Manifact*. 1934;13:271–276.
7. Nelson WL. Fouling of heat exchangers Part II. *Refin Nat Gas Manifact*. 1934;13:292–298.
8. Sileri D, Ding H, Sahu KC, Matar OK. Numerical simulations of immiscible two-fluid channel flow in the presence of phase change. In: *61st Annual Meeting of the American Physical Society, Division of Fluid Dynamics*. San Antonio, Texas; 2008.
9. Ishiyama EM, Coletti F, Macchietto S, Paterson WR, Wilson DI. Impact of deposit ageing on thermal fouling: lumped parameter model. *AIChE J*. 2010;56:531–545.
10. Crittenden BD, Kolaczkowski ST. Energy savings through the accurate prediction of heat transfer fouling resistances. In: O'Callaghan WO, ed. *Energy for Industry*. 1979;257–266.
11. Yeap BL, Wilson DI, Polley GT, Pugh SJ. Mitigation of crude oil refinery heat exchanger fouling through retrofits based on thermo-hydraulic fouling models. *Chem Eng Res Des*. 2004;82A:53–71.
12. Hewitt GF, Shires GL, Bott TR. *Process Heat Transfer*. London: CRC Press;1994.
13. Shah RK, Dusan PS. *Fundamentals of Heat Exchanger Design*. John Wiley & Sons, Inc;2003.
14. Yaglom AM, Kader BA. Heat and mass transfer between a rough wall and turbulent fluid flow at high Reynolds and Peclet numbers. *J Fluid Mech Digital Archive*. 1974;62:601–623.
15. Crittenden BD, Alderman NJ. Negative fouling resistances: The effect of surface roughness. *Chem Eng Sci*. 1988;43:829–838.
16. Albert F, Augustin W, Scholl S. Enhancement of heat transfer in crystallization fouling due to surface roughness. In: Müller-Steinhagen H, Malayeri R, Watkinson AP, eds. *EUROTHERM Heat Exchangers Fouling and Cleaning*. Schladming, Austria; June 14–19, 2009.
17. Bott TR. Fouling Notebook. *Institution of Chemical Engineers*; 1990.
18. Knudsen JG, Dahcheng L, Ebert WA. The determination of the threshold fouling curve for a crude oil. In: Bott TR, ed. *Understanding Heat Exchanger Fouling and its Mitigation*. Lucca, Italy: Begell House; 1997:265–272.
19. Wilson DI, Watkinson AP. Study of autoxidation reaction fouling in heat exchangers. *Can J Chem Eng*. 1996;74:236–246.
20. Asomaning S, Panchal CB, Liao CF. Correlating field and laboratory data for crude oil fouling. *Heat Transfer Eng*. 2000;V21:17–23.
21. Yeap BL, Wilson DI, Polley GT, Pugh SJ. Retrofitting crude oil refinery heat exchanger networks to minimize fouling while maximizing heat recovery. *Heat Transfer Eng*. 2005;26:23–34.
22. Kern DQ. *Process Heat Transfer*. New York: McGraw-Hill; 1988.
23. Yiantsios SG, Karabelas AJ. Fouling of tube surfaces: Modeling of removal kinetics. *AIChE J*. 1994;40:1804–1813.
24. Riazi MR. *Characterization and Properties of Petroleum Fractions*. 1st ed. Philadelphia: ASTM; 2005.
25. Coletti F, Macchietto S. A dynamic, distributed model of shell and tube heat exchangers undergoing crude oil fouling. *Submitted for publication*. 2009.
26. Coletti F, Macchietto S. Minimising efficiency losses in oil refineries: a heat exchanger fouling model. In: *Sustainable Energy UK: Meeting the Science and Engineering Challenge*. St Anne's College, Oxford, U.K; 2008.
27. Watkinson P. Critical Review of Organic Fluid Fouling: Final Report. *Argonne National Laboratory*; 1988.
28. Wilkes JO. *Fluid Mechanics for Chemical Engineers with Microfluidics and CFD*. 2nd ed. New York: Prentice Hall; 2005.
29. Gnielinski V. New equations for heat and mass-transfer in turbulent pipe and channel flow. *Int Chem Eng*. 1976;16:359–368.
30. Ebert WA, Panchal CB. Analysis of Exxon crude-oil-slip stream coking data. In: Panchal CB, ed. *Fouling Mitigation of Industrial Heat-Exchange Equipment*. San Luis Obispo, CA: Begell House Inc; 1995:451–460.
31. Panchal CB, Kuru WC, Liao CF, Ebert WA, Palen JW. Threshold conditions for crude oil fouling. In: Bott TR, ed. *Understanding Heat Exchanger Fouling and Its Mitigation*.: Lucca, Italy: Begell House; 1997:273–281.
32. Kern DQ, Seaton RE. A theoretical analysis of thermal surface fouling. *Br Chem Eng*. 1959;4:258–262.
33. Brown GG. *Unit Operations*. John Wiley & Sons; 1950.
34. Perry RH, Green DW. *Perry's Chemical Engineers' Handbook*. 7th ed. McGraw-Hill; 1997.
35. Yang M, Young A, Crittenden BD. Use of CFD to correlate crude oil fouling against surface temperature and surface shear stress in a stirred fouling apparatus. In: Müller-Steinhagen H, Malayeri R, Watkinson P, eds. *EUROTHERM Heat Exchangers Fouling and Cleaning*. Schladming, Austria, June 14–19, 2009.
36. Process Systems Enterprise. gPROMS. www.psenterprise.com/gproms. 1997–2009.
37. Macchietto S, Hewitt GF, Coletti F, Crittenden BD, Dugwell DR, Galindo A, Jackson G, Kandiyoti R, Kazarian SG, Luckham PF, Matar OK, Millan-Agorio M, Müller EA, Paterson W, Pugh SJ, SM. R, Wilson DI. *Fouling in Crude Oil Preheat Trains:* a Systematic Solution to an Old Problem. In: Müller-Steinhagen H, Malayeri R, Watkinson P, eds. *EUROTHERM Conference on Fouling and Cleaning in Heat Exchangers*. Schladming, Austria, June 14–19, 2009.

*Manuscript received Aug. 7, 2009, and revision received Feb. 8, 2010.*